Dephasing dynamics of an impurity coupled to an anharmonic environment

Max Bramberger and Inés De Vega

Department of Physics and Arnold Sommerfeld Center for Theoretical Physics, Ludwig Maximilian University Munich, 80539 Munich, Germany

(Received 6 August 2019; published 2 January 2020)

We analyze the dephasing dynamics of an impurity coupled to an anharmonic environment. We show that a strong anharmonicity produces two different effects depending on the environment temperature: For high temperatures, the system suffers a strong dephasing, while for low temperatures there is a strong information backflow (as measured by the Breuer-Laine-Piilo non-Markovianity measure). Both dephasing and backflow are particularly significant when the anharmonic potential allows environment states very close to the dissociation limit. In contrast, the information backflow is suppressed when assuming the environment to be Gaussian. In this regard, we find that the Gaussian approximation is particularly poor at low temperatures.

DOI: 10.1103/PhysRevA.101.012101

I. INTRODUCTION

An accurate description of hybrid systems such as molecular ensembles containing different types of degrees of freedom is still challenging. An often convenient approach is to consider some of these freedoms as an *open* system, while others that operate at a different timescale are treated as an environment and described by its statistical properties [1–6]. The open system may represent, for instance, an electronic component, while the environment describes a set of nuclei. In other situations the system is an impurity coupled to a complex environment that can be in condensed-matter form, a liquid, or a gas. One of the most successful approaches consists in approximating such an environment as a set of harmonic oscillators, an idea that was first put forward by Feynman and Vernon [7]. In this context, the best known model is the spin boson [8], which is extended to describe energy transfer between two or more molecules (or molecular states) in the presence of an environment [9,10]. Examples of these systems are antenna molecules within photosynthetic complexes that are coupled to a protein environment [11–16] or electron-transfer reactions between electronic donor and acceptor states that are conditioned by the motion of nuclear degrees of freedom [17–19]. In both cases, the protein and nuclear degrees of freedoms are represented by a harmonic bath producing dephasing. Other situations where electron transfer is affected by an environment include transport in polymers [20], the dynamics of organic molecules within solar cells [21], or impurities in strongly condensed matter or liquids [22].

However, the emergence of new scenarios and the rapid development of experimental techniques such as time-resolved nonlinear spectroscopy have given more information on the dynamics of complex molecular systems, therefore requiring more detailed models and analysis [23]. For instance, when the electronic dynamics occurs in the presence of nonpolar liquids or low-frequency intramolecular modes (such as torsional motion) the harmonic approximation is known to fail [17,24–28]. Also, nuclear environments may have a complex structure where some modes are highly anharmonic, while the remaining ones can be treated as harmonic and considered to be linearly coupled to the anharmonic ones [29,30]. Another relevant type of environment that is present in condensed-matter physics and quantum technological devices corresponds to a set of spins or spin bath [31]. For these spin environments it is well known that the statistics, i.e., the behavior of different order correlation functions of the environment coupling operators, is highly non-Gaussian, and therefore their description in terms of a spectral density is highly inaccurate. In such a context of quantum technological devices, where noise-optimized quantum control is required, an accurate characterization of the environment and its non-Gaussian features is essential [32,33].

In this paper we consider an impurity coupled to an environment consisting of a set of independent Morse oscillators [34,35] producing dephasing. Advantageously, the Morse oscillator Hamiltonian is analytically solvable [36], giving rise to a spectrum of discrete energy levels, or bound states, and a set of scattering states. Such scattering states form a continuum that produces an additional decoherence and is describable as a harmonic bath [37,38]. Here we are not interested in a complete description of the whole Morse spectrum but rather focus on its discrete part. This allows us to make a systematic study of the effects of the anharmonicity on the open-system dynamics: By tuning the anharmonicity of the potential we will be able to vary from a regime where each environment oscillator has a large number of equally spaced bound states, thus a harmonic limit, to a highly anharmonic situation with only two bound states. In other words, our model allows us to describe the dephasing dynamics of an impurity coupled to a harmonic bath and to a spin bath, as well as all the intermediate anharmonic regimes. As shown in Fig. 1, the Hamiltonian describes a star configuration, with the impurity coupled to a set of independent oscillators such that the harmonic and spin limits correspond to the pure dephasing version of the spin-boson and central spin models, respectively.

The paper is organized as follows. We first discuss general concepts of the model in Sec. II as well as the dynamical map

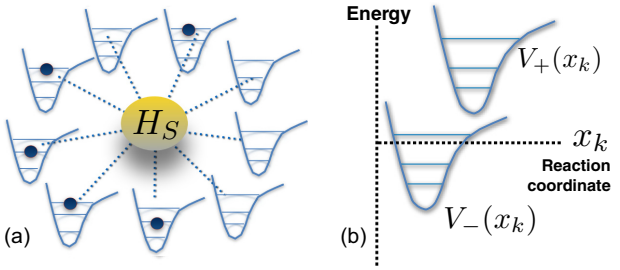

FIG. 1. (a) Scheme of the open quantum system coupled to an environment of anharmonic oscillators, which we model with a Morse potential. (b) Schematic of the upper and lower level energy potential surfaces in one of the multidimensional reaction coordinates x_k that describes an energy-transfer reaction between the electronic levels $|+\rangle$ and $|-\rangle$.

that describes the reduced dynamics of the impurity. Then we divide the analysis into three parts. In Sec. III we discuss the changes in the impurity dephasing time, which is intimately related to the persistence of quantum-mechanical properties such as coherence and entanglement along the evolution, when considering two impurities initially entangled [39]. In Sec. IV we consider the ratio between the flow of information towards and away from the impurity [40], which determines the amount of information that is lost from the system into the environment. In turn, such a ratio is strongly linked to the presence of Breuer-Laine-Piilo non-Markovianity [4,5,41], a concept that has gained increasing attention in various contexts including quantum information and quantum metrology, biological systems, ultracold atoms, or quantum thermodynamics [6]. In Sec. V we analyze the degree to which the impurity dynamics can be well described with a Gaussian map such that it only depends on the environmental second-order moment or correlation function. This will allow us to explore when the non-Gaussianity of the environment becomes more or less relevant depending on the environment temperature and the anharmonicity parameter. Finally, in Sec. VI we draw some conclusions and provide an outlook for future work.

II. A SPIN COUPLED TO A MORSE OSCILLATOR ENVIRONMENT

We consider a system with a total Hamiltonian $H = H_S + H_E + H_I$. This corresponds to an impurity with the Hamiltonian ($\hbar = 1$)

$$H_S = \omega_s \sigma_z, \tag{1}$$

where σ_z is a spin ladder operator that can be written in terms of the impurity internal basis $|\pm\rangle$ as $\sigma_z = |+\rangle\langle+| - |-\rangle\langle-|$, coupled to an anharmonic environment composed of independent harmonic oscillators with a Hamiltonian $H_E = \sum_k H_k$ ($k \in \{1, \ldots, 40\}$), where

$$H_k = \frac{p_k^2}{2m} + D_k(e^{-2\alpha_k x_k} - 2e^{-\alpha_k x_k}) \tag{2}$$

describes each kth oscillator in terms of a Morse potential. Here we have defined the position operator as $x_k = \sqrt{\alpha_k/2m\omega_k}(b_k + b_k^\dagger)$, where b_k ($b_k^\dagger$) is the standard harmonic annihilation (creation) operator. The depth and the width of the Morse potential is determined by two different parameters D_k and α_k, respectively. Notice that this represents a specific case of Fig. 1(b) in which the potential part $V(x_k) = D_k(e^{-2\alpha_k x_k} - 2e^{-\alpha_k x_k})$ is centered at the origin and equal for both impurity levels. Finally, the coupling is described through the Hamiltonian

$$H_I = S \otimes B, \tag{3}$$

where $S := \sigma_z$ and B are the system and environment coupling operators, respectively. Just like for the free Hamiltonian, we can write $B = \sum_k B_k$, where

$$B_k = g_k(b_k + b_k^\dagger), \tag{4}$$

with g_k a constant that determines the coupling strength of the kth oscillator to the system. Thus, we consider the coupling as linear and therefore proportional to the position operator (also called reaction coordinate in the context of electron transfer) of each Morse oscillator $B_k \sim x_k$ [19,23,26–28,42].

A. Properties of the Morse potential

Proposed in [36], the Morse potential was one of the first empirical models to describe anharmonicities in the vibration of diatomic molecules and is now widely used to describe complex anharmonic effects [34,35,42]. The Morse potential presents various interesting features. First of all, it is analytically solvable, yielding a finite number of bound states with negative energies given by

$$E_{kn} := -\frac{\omega_k \Lambda}{2} - \frac{\omega_k}{2\Lambda}\left(n + \frac{1}{2}\right)^2 + \omega_k\left(n + \frac{1}{2}\right). \tag{5}$$

These energies depend on the depth and the width of the potential through a new parameter Λ such that $D_k = \frac{\omega_k \Lambda}{2}$ and $\alpha_k = \sqrt{\frac{\omega_k}{\Lambda}}$. Thus, ω_k is the frequency of the harmonic part of the potential, while the parameter Λ tunes the anharmonic component. Note that while we consider the same anharmonicity parameter for all environment oscillators, their frequencies are linearly distributed.

Besides the bound states, the Morse potential presents a continuous spectrum of positive-energy eigenstates, also known as scattering states, which will not be considered here for simplicity. Overall, they will correspond to a continuous bath of free particles, to which the impurity may be coupled too and which may produce additional dephasing. In the new eigenstate basis, with the nth energy eigenstate of the kth oscillator written as $|kn\rangle$ and the respective eigenenergies E_{kn}, we find that Eqs. (2) and (4) can be written as

$$H_k = \sum_n E_{kn}|kn\rangle\langle kn|, \tag{6}$$

$$B_k = \sum_{n,m} c_{nm}^k |kn\rangle\langle km|, \tag{7}$$

where $c_{nm}^k = \langle kn|B_k|km\rangle$ are the coefficients for the bath part of the interaction operator.

A second interesting property is that the number of bound states is uniquely given by the integer part of $\Lambda + \frac{1}{2}$, when $\Lambda + \frac{1}{2}$ is not an integer. When $\Lambda + \frac{1}{2}$ is an integer, the number of bound states is $\Lambda - \frac{1}{2}$. This allows us to tune, by simply varying Λ, our bath between a spin bath limit,

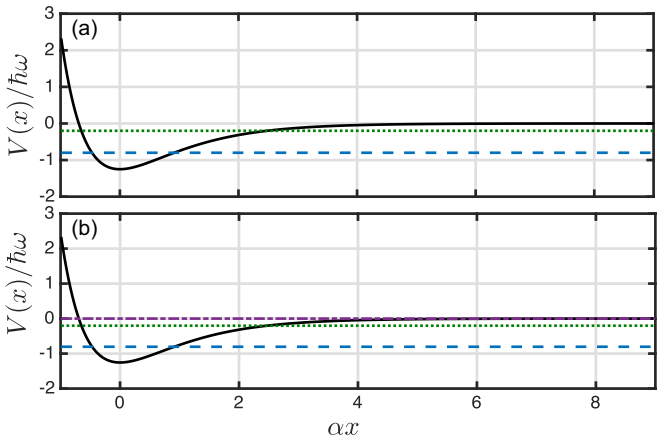

FIG. 2. Morse potential and eigenvalues of the bound states for different values of the anharmonic parameter: (a) region I, $\Lambda \equiv \Lambda^{n=2,\epsilon=0} = 2.5$, displaying two bound states far from the dissociation limit, and (b) region II, $\Lambda \equiv \Lambda^{n=2,\epsilon=0.1} = 2.51$, giving rise to the same bound states and a third one that corresponds to a weakly bounded state, close to the dissociation limit.

corresponding to $\Lambda \in]\frac{3}{2}, \frac{5}{2}]$, to a harmonic limit, recovered for $\Lambda \to \infty$. Note that at $\frac{3}{2}$ the Morse oscillator has only one bound state. Between these limits, we also find two different types of regions in Λ which will determine the nature of the dynamics: type I regions where all environment states are strongly bounded, corresponding to $\Lambda \equiv \Lambda^{n,-\epsilon} = n + \frac{1}{2} - \epsilon$, with n an integer and $0 \leqslant |\epsilon| \ll 1$ a real number, and type II regions where a new bound state is formed, which moreover is weakly bounded, corresponding to $\Lambda \equiv \Lambda^{n,\epsilon} = n + \frac{1}{2} + \epsilon$, with n an integer and $0 < \epsilon \ll 1$ a positive real number. A typical situation in both regions can be observed in Fig. 2 for the case of $n = 2$, when choosing $\epsilon = 0$ (region I) and $\epsilon = 0.1$ (region II).

B. Properties of the open-system dynamics

We now consider an initially decorrelated state so that the total density operator is written as $\rho(t=0) = \rho_0 \otimes \rho_E^\beta$, where ρ_0 is the initial state of the system, and the environment is in a thermal equilibrium $\rho_E^\beta := e^{-\beta H_E}/\mathrm{Tr}_E\{e^{-\beta H_E}\}$, with the inverse temperature $\beta = 1/k_B T$ and k_B the Boltzmann constant. In the general case, the reduced density matrix of the system in the interaction picture can be written as

$$\rho_s(t) = \mathrm{Tr}_E\left\{\mathcal{U}^{-1}(t,t_0)\rho_s(0)\otimes\rho_B^\beta(0)\mathcal{U}(t,t_0)\right\}, \tag{8}$$

where $\mathcal{U}(t,t_0)$ is the evolution operator in the interaction picture, which can be expanded with a Dyson series as

$$\mathcal{U}(t,t_0) = 1 - i\int_{t_0}^{t} dt_1 H_I(t_1) + (-i)^2\int_{t_0}^{t} dt_1\int_{t_0}^{t_1} dt_2 H_I(t_1)H_I(t_2) + \cdots. \tag{9}$$

Considering this expansion as well as the case $H_I = SB$, we find that the time evolution of $\rho_s(t)$ can be rewritten in terms of an infinite series of lth-order correlation functions which at zero time have the general form

$$C^l(0) = \mathrm{Tr}_E\{B^l\rho_E\} = \sum_{k_1,\ldots,k_l}\mathrm{Tr}_E\left\{B_{k_1}\cdots B_{k_l}\rho_E\right\}. \tag{10}$$

Here the sum covers all configurations of $\{k_1,\ldots,k_l\}$ and can be decomposed into sums over sectors where different numbers of those k coincide. As noted above, our model describes a linear system-environment coupling such that for each oscillator $B_k \sim x_k$, with x_k the position operator. Three important consequences can be extracted from such linear coupling to an anharmonic environment.

(i) The first-order term ($l = 1$) in the expansion (10) needed to recover Eq. (8) is nonzero. This is because the coupling is linear and the environment Hamiltonian describes an asymmetric potential such that $\langle B\rangle_E^\beta := \mathrm{tr}_B\{B\rho_E^\beta\} \neq 0$. This fact can be remedied by considering a renormalized version of the Hamiltonian such that $H = \tilde{H}_S + H_E + \tilde{B}\sigma_z$, where $\tilde{H}_S = \omega_s\sigma_z + \sigma_z\langle B\rangle_E^\beta$ and $\tilde{B} = B - \langle B\rangle_E^\beta$. Hence, the correlations involved in Eq. (8) are equal to the ones in Eq. (10) but replacing each B_k by their renormalized counterpart $\tilde{B}_k$.

(ii) After the first-order term, the most important contribution, i.e., the second-order term or correlation function

$$\alpha(t-s) = \mathrm{Tr}_E\left\{\tilde{B}(t)\tilde{B}(s)\rho_E^\beta\right\}, \tag{11}$$

has a real part that does not decay to zero at finite temperatures but to a constant positive value. In terms of the eigenvalues and eigenvectors of the environment $\{E_{kn}, |kn\rangle\}$, the correlation function (11) can be formally written as $\alpha(t) = C(t) + C^0$, where

$$C^0 = \sum_{k,n}|\langle kn|\tilde{B}_k|kn\rangle|^2\frac{e^{-\beta E_{kn}}}{Z_k} \tag{12}$$

corresponds to an offset, while

$$C(t) = \sum_k\sum_{p\neq n}|\langle kn|\tilde{B}_k|kp\rangle|^2\frac{e^{-\beta E_{kn}}}{Z_k}e^{i\Delta_{np}^k t} \tag{13}$$

corresponds to a time-dependent component, where we have defined $\Delta_{np}^k = E_{kn} - E_{kp}$. When we have a sufficiently large number of interfering phases, such a time-dependent factor decays. However, the time-independent contribution will produce a real offset that will only be canceled in the zero-temperature limit, i.e., when we have that $C^0 = \sum_k|\langle k0|\tilde{B}_k|k0\rangle|^2 = |\langle\tilde{B}\rangle_E^\infty|^2 = 0$.

(iii) The offset is particularly important in regions of type II, i.e., for values of Λ for which a weakly bound state exists, since these correspond to highly asymmetric bound states leading to a large overlap $\langle km|\tilde{B}_k|km\rangle$, where we define m as the index of such a weakly bound state. The presence of the weakly bounded state has two important consequences. First, it holds that

$$\lim_{\varepsilon\to 0^+}\langle m|x|m\rangle = \ln(2m+1) - \lim_{\varepsilon\to 0^+}\psi(2\varepsilon) - \psi(1) + \psi(m+1) = \infty, \tag{14}$$

where we have just inserted the matrix element given in (B28) and took the limit. In consequence, the offset becomes very large near such limit and when the temperature is high enough so as to have a large initial population in the upper energy

level. The second consequence is that all the transitions to the bound state with highest energy are suppressed. To show this, we consider a bound state $|l\rangle$ having energy lower than $|m\rangle$, when

$$\lim_{\varepsilon\to 0^+}\langle l|x|m\rangle = \frac{2(-1)^{m-l+1}}{(m-l)(m-l)} \times\sqrt{\frac{m!(m-l)\Gamma(m+1)}{l!\Gamma(2m-l+1)}}\lim_{\varepsilon\to 0^+}\sqrt{\varepsilon}=0. \quad (15)$$

Here we took (B29), inserted $N = m+\varepsilon$, and used that the functions containing ε are continuous functions so we could pull the limit into them. The consequence is that the time-dependent term of the correlation function, given by Eq. (13), is not affected by the presence of the bound state, contrary to the offset part.

(iv) So far we have focused on the first- and the second-order moments of the expansion (10). However, in the present anharmonic case the structure of such an expansion is much richer than in the harmonic case. First, the terms in $\mathrm{Tr}_E\{\tilde{B}_{k_1}\cdots\tilde{B}_{k_l}\rho_E\}$ having an odd number of identical k_j no longer vanish, that is, $\mathrm{Tr}_E\{\tilde{B}_k^{2n+1}\cdots\tilde{B}_k\rho_E\}\neq 0$ when n is an integer. Moreover, the even-order components can no longer be decomposed as products of second-order components of the form (11). Naturally, these two properties are fulfilled in the harmonic bath case, leading to system dynamical equations that can be written solely in terms of the correlation function (11). Indeed, Wick's theorem holds in the harmonic case, since there H_k is quadratic and one can decompose $B_k(t) = e^{iH_kt}B_ke^{-iH_kt} = f_k(t)b_k(0) + f_k^*(t)b_k^\dagger(0)$ [with $f_k(t)$ a time-dependent function]. Away from this limit, such a decomposition is no longer possible and Wick's theorem can no longer be applied.

One way to diminish the relative weight of higher-order terms with respect to the second-order one (11) is to choose an appropriate scaling for the coupling strengths g_k present in the environment coupling operators B_k. In detail, if we choose them to scale as $g_k\sim 1/\sqrt{K}$, where K is the number of oscillators, it can be shown that higher-order correlations will eventually vanish in the limit of large K, an idea that was originally proposed in [43] and that is further discussed in [44].

In our case, we consider a fixed number of oscillators $K = 40$ and explore to what extent the higher-order terms are relevant to the description of the system. In order to be consistent with the harmonic-oscillator limit, we further consider the standard choice in this limit for the frequency distribution and coupling strengths

$$\omega_k := \frac{2\omega_c}{K}k, \quad (16)$$

$$g_k := \sqrt{\frac{2\omega_c}{K}J(\omega_k)}. \quad (17)$$

Here $J(\omega)$ is the spectral density, which we consider to be of Ohmic type

$$J(\omega) := \Theta(2\omega_c-\omega)\eta\frac{\omega}{\omega_c}e^{-\omega/\omega_c}, \quad (18)$$

with a special hard cut; ω_c is a cutoff frequency and η is a parameter with which we modulate the strength of the system-environment coupling. For the harmonic case, the chosen linear discretization $\omega_k = k\Delta\omega$, with $\Delta\omega = 2\omega_c/K$, gives rise to a revival time (which is the time at which finite-size effects of the environment will start to occur) which in our case is $T = \pi/\Delta\omega\approx 20$.

C. Dynamical map

Because we are considering pure dephasing, we have that $[H_S, S] = 0$, which implies that the Hamiltonian is in block-diagonal form and can be written as

$$H = P_+\left(\omega_s+\sum_k H_k^+\right)+P_-\left(-\omega_s+\sum_k H_k^-\right), \quad (19)$$

where we have defined the projectors $P_\pm := |\pm\rangle\langle\pm|$ in terms of the eigenstates $|\pm\rangle$ of σ_z with eigenvalues ±1 and we have decomposed both H_E and B in terms of local operators $H_k^\pm := H_k\pm B_k$, with H_k corresponding to the kth oscillator. Thus, the time-evolution operator can be computed as

$$e^{iHt} = P_-e^{-i\omega_st}\prod_k e^{iH_k^-t}+P_+e^{i\omega_st}\prod_k e^{iH_k^+t}. \quad (20)$$

To obtain this expression, we have used the fact that the two terms in (19) commute, as well as the locality of the terms in the exponential to factorize it. Thus, computing Eq. (20) requires only having to exponentiate local operators, which can be done efficiently. Indeed, the total Hilbert space dimension scales like d^K, where d is the local dimension, and we only have to exponentiate matrices of size d. Thus, the total density operator $\rho(t) = e^{-iHt}\rho_0\otimes\rho_E^\beta e^{iHt}$ can be rewritten as

$$\begin{aligned}\rho(t) = {}& P_+\rho_0P_+\otimes e^{-iH^+t}\rho_E^\beta e^{iH^+t}\\ &+P_-\rho_0P_-\otimes e^{-iH^-t}\rho_E^\beta e^{iH^-t}\\ &+P_-\rho_0P_+\otimes e^{-iH^-t}\rho_E^\beta e^{iH^+t}e^{2i\omega_st}\\ &+P_+\rho_0P_-\otimes e^{-iH^+t}\rho_E^\beta e^{iH^-t}e^{-2i\omega_st}, \end{aligned}\quad (21)$$

where we have defined $H^\pm := \sum_k H_k^\pm$. Taking the partial trace over the bath degrees of freedom yields the reduced density matrix of the system, which has the form

$$\rho_s(t) = \Phi(t)[\rho_s(0)] = \begin{pmatrix}\rho_s^{11}(0) & \chi(t)\rho_s^{12}(0)\\ \chi^*(t)\rho_s^{21}(0) & \rho_s^{22}(0)\end{pmatrix}, \quad (22)$$

where we have defined the decaying factor as

$$\chi(t) = e^{2i\omega_st}\prod_k \mathrm{tr}_k\left(e^{-iH_k^-t}\rho_k^\beta e^{iH_k^+t}\right), \quad (23)$$

where ρ_k^β is the thermal state of the kth oscillator with respect to its free Hamiltonian. We note that despite the presence of an offset (12) which gives rise to an ill-defined weak-coupling master equation, we have numerically found that the map (23) is invertible for all the parameter regimes we have considered here (not shown), which suggests that a time-local master equation is still well defined [45].

Harmonic and spin limits

In the harmonic-oscillator limit, the decay factor acquires the usual form

$$\chi(t) = e^{2i\omega_s t - \Gamma(t)}, \tag{24}$$

where

$$\Gamma(t) := 8\sum_k \frac{g_k^2}{\omega_k^2}\sin^2\left(\frac{\omega_k t}{2}\right)\coth\left(\frac{\beta\omega_k}{2}\right)$$
$$= 4\,\mathrm{Re}\left\{\int_0^t ds\int_0^s du\,\alpha(s-u)\right\}, \tag{25}$$

with $\alpha(t-s) = \mathrm{Tr}_E\{\tilde{B}(t)\tilde{B}(s)\rho_E^\beta\}$. Moreover, note that in the harmonic limit $\tilde{B} = B$, since $\langle B\rangle^\beta = 0$. In addition, the offset (12) of the correlation function vanishes.

In the opposite limit of a spin bath, i.e., when $1.5 < \Lambda \leqslant 2.5$, the operators H_k and B_k can be written in terms of the Pauli matrices σ_j^k, which are elements of the vector $\vec{\sigma}_k = (\mathbb{1}_k, \sigma_x^k, \sigma_y^k, \sigma_z^k)$, where we have defined the first element $\sigma_0^k = \mathbb{1}_k$ in terms of the unit operator in the Hilbert space of the kth oscillator. In this representation we find that

$$H_k^+ = \vec{c}_k\cdot\vec{\sigma}_k, \quad H_k^- = \vec{d}_k\cdot\vec{\sigma}_k, \tag{26}$$

where each component of $\vec{c}_k$ and $\vec{d}_k$ is defined as $c_j^k = \frac{1}{2}\mathrm{Tr}_k(H_k^+\sigma_j^k)$ and $d_j^k = \frac{1}{2}\mathrm{Tr}_k(H_k^-\sigma_j^k)$, respectively. Thus, the exponentials appearing in Eq. (23) can be simplified as

$$e^{\pm iH_k^+ t} = \left(\mathbb{1}\cos(\|\vec{c}_k\|t) \pm i\frac{\vec{c}_k\cdot\vec{\sigma}_k}{\|\vec{c}_k\|}\sin(\|\vec{c}_k\|t)\right)e^{\pm ic_0^k t},$$
$$e^{\pm iH_k^- t} = \left(\mathbb{1}\cos(\|\vec{d}_k\|t) \pm i\frac{\vec{d}_k\cdot\vec{\sigma}_k}{\|\vec{d}_k\|}\sin(\|\vec{d}_k\|t)\right)e^{\pm id_0^k t}. \tag{27}$$

III. DEPHASING TIME

We first analyze the dephasing time of the system, i.e., the decaying of the off-diagonal elements of the reduced density matrix. For all the numerical results we choose frequency units of $\omega_s = 1$. Moreover, we consider the initial state

$$\rho_0 = \tfrac{1}{2}\left(\mathbb{1} + \tfrac{1}{2}\sigma_x\right). \tag{28}$$

Although this choice is rather arbitrary, it ensures that there are initial coherences that allow us to analyze dephasing. In other words, our analysis is independent of the initial condition as long as it contains coherences. We define the decay time τ_d as the time such that

$$\frac{|\langle 0|\rho_S(\tau_d)|1\rangle|}{|\langle 0|\rho_S(t=0)|1\rangle|} = \frac{1}{10}, \tag{29}$$

with the reduced density matrix given by Eq. (22).

Figures 3(a) and 3(b) display the decay time τ_c for different values of the anharmonicity parameter Λ and different initial temperatures of the bath. For the following discussion it is important to remember that as Λ increases, the anharmonicity decreases. In detail, in Fig. 3(a) we explore the values of $\Lambda \equiv \Lambda^{n,\epsilon=0} = n + \frac{1}{2}$, which correspond to type I regions where the highest-energy bound state is as far as possible from the dissociation limit, i.e., as strongly bounded as possible. With this choice, we find that τ_c has a quite smooth behavior with

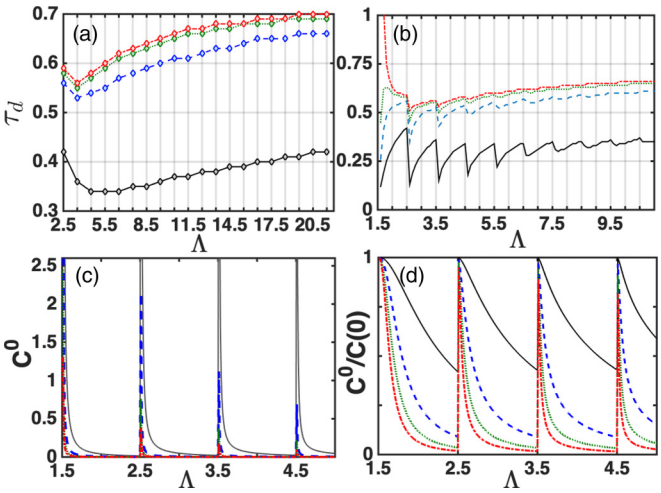

FIG. 3. (a) and (b) Dephasing rate for a coupling strength of $\eta = 2$ in Eq. (18), with (a) low resolution with values of Λ separated by a step $\delta\Lambda = 1$ and (b) high resolution with $\delta\Lambda = 0.1$. Also shown are (c) the offset and (d) relative value of the offset $C^0/C(t=0)$, for high resolution $\delta\Lambda = 0.01$ and $\eta = 0.01$. All panels display the curves for different inverse temperatures $\beta = 1, 4, 7, 10$ corresponding to black solid, blue dashed, green dotted, and red dot-dashed lines, respectively.

the anharmonicity, displaying a general tendency to increase towards the harmonic limit. Such a trend reverses towards higher anharmonicities, where the number of bound states becomes increasingly limited and the dephasing slows down again.

As shown in Fig. 3(b), such a smooth behavior is disrupted when including a finer grid of Λ values, now taking closer points spaced by $\delta\Lambda = 0.1$. One can clearly identify that the regions of type I end up with a peak at values $\Lambda = n + \frac{1}{2}$ [where the top of the peaks corresponds to the points shown in Fig. 3(a), followed by a dip at values $\Lambda^{n,\epsilon}$ with ϵ very small, i.e., when the type II regions begin. Indeed, as discussed in Fig. 3(a), at high anharmonicities each oscillator has only a few energy levels, which in principle hinders the dephasing. However, when entering each type II region a new bound state is formed, and the offset becomes so large that it compensates for this effect and leads to a strong dephasing.

Another interesting feature of the figure is that in the spin region the decay time goes to infinity at low temperatures and at low ε at the beginning of region II. Indeed, we have seen in Eq. (15) that all the transitions to the bound state with the highest energy are suppressed in type II regions. Thus, when we only have two bound states, the limit $\varepsilon \to 0$ gives rise to bath operators $H_k^\pm$ that are diagonal. To see this, we find that for $\Lambda = 1.5 + \varepsilon$ and small ε,

$$\lim_{\varepsilon\to 0^+} c_x^k = \lim_{\varepsilon\to 0^+}[\mathrm{tr}_k(H_k^+\sigma_x) - \mathrm{tr}_k(B_k\sigma_x)] = 0,$$
$$\lim_{\varepsilon\to 0^+} c_y^k = \lim_{\varepsilon\to 0^+}[\mathrm{tr}_k(H_k^+\sigma_y) - \mathrm{tr}_k(B_k\sigma_y)] = 0, \tag{30}$$

and similarly $\lim_{\varepsilon\to 0^+} d_x^k = 0$ and $\lim_{\varepsilon\to 0^+} d_y^k = 0$. In addition,

$$c_z^k = \mathrm{tr}_k(H_k^+\sigma_z) + \mathrm{tr}_k(B_k\sigma_z),$$
$$d_z^k = \mathrm{tr}_k(H_k^-\sigma_z) - \mathrm{tr}_k(B_k\sigma_z), \tag{31}$$

and their limit $\varepsilon \to 0^+$ will diverge as predicted by the general case (14). If we now consider Eqs. (27) for a very small ε and ignore for this argument the phase that comes from the c_0 and the d_0 contribution because it does not affect the absolute value of the coherences, we find

$$\lim_{\varepsilon\to 0^+} e^{\pm iH_k^+ t} = \mathbb{1}_k \cos(\phi_k^+ t) \pm i\sigma_z \sin(\phi_k^+ t),$$
$$\lim_{\varepsilon\to 0^+} e^{\pm iH_k^- t} = \mathbb{1}_k \cos(\phi_k^- t) \mp i\sigma_z \sin(\phi_k^- t), \quad (32)$$

where we have defined the phases $\phi_k^+ = \lim_{\varepsilon\to 0^+} \|\vec{c}_k\|$ and $\phi_k^- = \lim_{\varepsilon\to 0^+} \|\vec{d}_k\|$. Strictly speaking, the above equations are ill-defined in the limit $\lim_{\epsilon\to 0}$. For this reason, we look at small but not infinitesimal ϵ. Also, we note that the sign between the two terms in the second of Eqs. (32) is flipped as compared to the first. This is because the $\mathrm{tr}_k(H_k\sigma_z)$ term in Eq. (31) becomes insignificant compared to the $\mathrm{tr}_k(B_k\sigma_z)$ term. The phases $\phi_k^\pm$ are going to infinity in the limit $\varepsilon \to 0^+$. However, if we stay at a very small yet not tiny value of ε we can consider that $\phi_k^\pm \approx \Gamma^\pm$, where $\Gamma^\pm$ are two large phases, and define $\Gamma_T = \Gamma^- + \Gamma^+$ such that in Eq. (23) we now have

$$\mathrm{tr}_k\left(e^{-iH_k^- t}\rho_k^\beta e^{iH_k^+ t}\right) \approx \cos(\Gamma_T t) + i\sin(\Gamma_T t)\mathrm{tr}_k(\sigma_z\rho_k), \quad (33)$$

where $\mathrm{tr}_k(\sigma_z\rho_k) = \tanh(\frac{\beta\Delta E_k}{2})$, with ΔE_k the energy difference of the kth spin. Thus, at zero temperature we simply find

$$\left|\mathrm{tr}_k\left(e^{-iH_k^- t}\rho_k^\beta e^{iH_k^+ t}\right)\right| \approx \cos^2(\Gamma_T t) + \sin^2(\Gamma_T t) = 1. \quad (34)$$

The reason why the dephasing time does not increase to infinity at the beginning of other type II regions in the plot is because as soon as there are more bound states some off-diagonal transitions to intermediate states are allowed, which gives rise to dynamics even in the zero-temperature case.

The large offset at the beginning of type II regions can be observed in Fig. 3(c), and as argued before in point (iii) it is particularly relevant at high temperatures. From this plot, one may be tempted to believe that the offset is only important in such regions of type II. However, from the representation in Fig. 3(d) one can see that relative value of the offset with respect to the maximal value of the time-dependent part, i.e., $C^0/C(t=0)$, is non-negligible in all regions of Λ, including region I, where there is no weakly bounded state. Thus, on the one hand, the offset explains the short dephasing time at high temperatures ($\beta = 1$) with respect to lower temperatures and, on the other hand, for all temperatures it explains the tendency for a shorter dephasing towards smaller Λ.

IV. OUTFLOW AND BACKFLOW OF INFORMATION

We now analyze how the outflow and backflow of information are affected by the degree of anharmonicity of the environment. To this aim, we consider that the backflow of information, as obtained from the Breuer-Laine-Piilo measure, can be written as [40]

$$\mathcal{N}_- = \sum_n |\chi(t_{2n})| - |\chi(t_{1n})|, \quad (35)$$

where $[t_{1n}, t_{2n}]$ are the time intervals over which $|\chi(t))|$ increases and $\chi(t)$ is given by Eq. (23). In a similar way

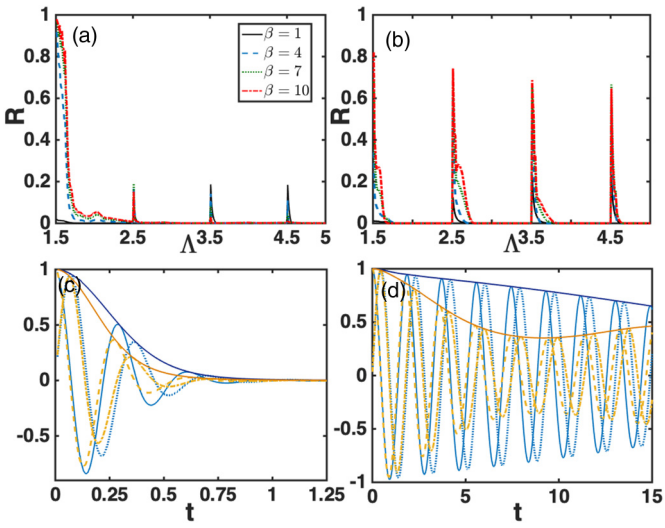

FIG. 4. Rate (36) for (a) strong coupling $\eta = 2$ and (b) weak coupling $\eta = 0.01$. Also shown is the evolution of $\chi(t)$ in Eq. (23) for $\beta = 7$ and (c) strong coupling $\eta = 2$ and (d) weak coupling $\eta = 0.01$. The oscillatory blue solid and dotted lines correspond to the real and imaginary parts of $\chi(t)$ for $\Lambda = 2.5$, while the yellow dashed and dot-dashed lines correspond to the real and imaginary parts for $\Lambda = 2.6$, respectively. Solid lines in the peaks represent the corresponding $|\chi(t)|$.

as in [40], we consider the ratio between the information backflow, given by Eq. (35), and the analogous quantity corresponding to the information flow to the environment $\mathcal{N}_+$,

$$R = \mathcal{N}_-/\mathcal{N}_+. \quad (36)$$

Figure 4(a) represents the ratio R for different values of anharmonicity Λ and for the same coupling value ($\eta = 2$) considered in the dephasing time analysis. We find that the only region where there is a non-negligible backflow of information is the highly anharmonic one, particularly the spin-bath region. Figure 4(b) represents the same quantity but for weaker coupling $\eta = 0.01$, showing that in this case the backflow of information is also significant for higher values of Λ, particularly near the transition regions where a new environment bound state has been formed. Interestingly, the presence of backflow is related to the following features.

(i) At high temperatures there is almost no backflow. As seen before, the presence of a large offset gives rise to a fast dephasing time, which in turn eliminates any possibility of backflow and therefore non-Markovianity.

(ii) At lower temperatures, the offset is not as important as to eliminate all the structure in the dephasing dynamics, and the maximal backflow is observed precisely at the same values of Λ where a new bound state has just been created (regions II).

The dynamics of $\chi(t)$ can be observed in Figs. 4(c) (strong coupling) and 4(d) (weak coupling) for $\beta = 7$. In detail, one can observe that while the real and imaginary parts of $\chi(t)$ are oscillatory, its absolute value is a monotonically decreasing function for $\Lambda = n + 0.5 = 2.5$ and becomes nonmonotonically decreasing, i.e., giving rise to backflow, for $\Lambda = 2.6$, i.e., for a Morse potential value having a weak bound state.

An important comment is in order here. Since our environment is finite, a border effect is to be expected at a certain time. For $K = 40$ oscillators, the revival time can be estimated to be $T = 20$ in the harmonic limit (see [46] and references therein for details), but it is much harder to compute in the anharmonic case. The reason is that, while in the harmonic case the revival time is the time at which the correlation function, having decayed, starts to grow again, in the anharmonic case we have seen that such a function is not the only one that comes into play. For $\eta = 2$ the system off-diagonal elements have already decayed to zero at all values considered, which allows us to consider our analysis of dephasing time. However, this is not the case for smaller values, such as $\eta = 0.01$, where at $T = 20$ there are curves that have not yet decayed. This means that the present analysis of forward flow and backflow has been performed within a time frame up to $T = 20$, where we can neither consider that the system has always completely decayed nor exclude border effects in the anharmonic limit. A rigorous analysis of such finite-size effects produced by nonharmonic environments is beyond the present scope, but would be very interesting. In particular, it is interesting to ask whether the measured backflow is due to such finite-size effects or to the nature of the environment itself, as considered in the harmonic case.

Finally, we computed the non-Markovianity by considering the Gaussian map $\chi^{\text{Gauss}}(t)$ given by Eq. (24) and the correlation function (11), finding that it is zero for all parameter regimes considered. It remains to be further analyzed if Gaussian evolutions (or their related properties such as non-Markovianity) obey some extremality property like that of Gaussian states [47].

V. NON-GAUSSIAN NATURE OF THE BATH

We have seen in the previous sections that near the limit where a weakly bounded upper state is present in the environment oscillators there is a strong information backflow, particularly at low temperatures. In this section we will further explore the nature of such non-Markovianity and show that it is linked to a strong non-Gaussianity of the bath. To this aim, we will compare the map (22) computed with the exact non-Gaussian $\chi(t)$ corresponding to the Morse environment (23) with the Gaussian $\chi^{\text{Gauss}}(t)$ [again as given by Eq. (24) with the correlation function (11)]. Doing so, we are comparing the exact dynamics with that obtained by assuming that the map is Gaussian, and therefore fully determined by the second-order moment. The density plot in Fig. 5 shows the error $E(t) = |\chi(t) - \chi^{\text{Gauss}}(t)|$ for low [Fig. 5(a)] and high [Fig. 5(b)] temperatures, for different times and anharmonicities. It can be observed in general that the Gaussian map becomes a particularly bad approximation in the regions near the formation of a new bound state (but not only) and at low temperatures. This behavior can be best observed in Fig. 6, which represents the time-averaged error

$$E = \frac{1}{T}\int_0^T ds\, D\big(\rho_s(t), \rho_s^{\text{Gauss}}(t)\big), \tag{37}$$

where $\rho_s(t)$ represents the exact evolution, $\rho_s^{\text{Gauss}}(t)$ is the Gaussian-approximated evolution as given by $\chi^{\text{Gauss}}(t)$, and $D(A, B) = \frac{1}{2}\text{Tr}\{\sqrt{(A-B)^2}\}$ represents the trace distance

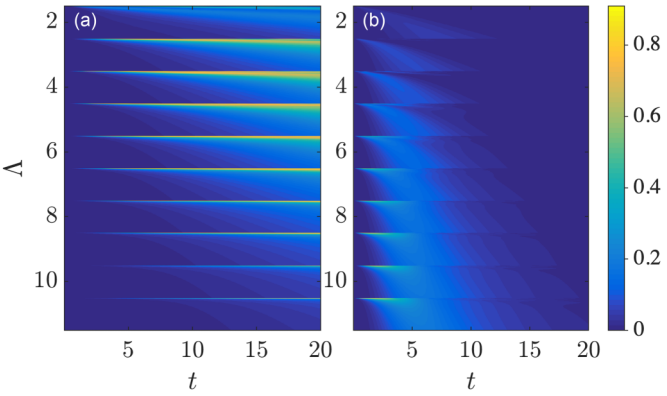

FIG. 5. Density plot of $E_\chi(t) = |\chi(t) - \chi^{\text{Gauss}}(t)|$ for (a) $\beta = 10$ and (b) $\beta = 1$.

between the two density matrices A and B. It can be observed that the error is large for all temperatures explored except for very high values ($\beta = 1$). We note that in the scale that we show it seems to increase slightly with Λ. This is a local effect which disappears, as expected, when going further to the harmonic limit. Figures 6(b) and 6(c) show how the emergence of a new bound state (for $\Lambda = 2.6$) gives rise to a strong departure of the Gaussian approximation with respect to the exact case.

VI. CONCLUSION

We have analyzed the dephasing dynamics of an impurity coupled to an environment of oscillators containing a varying

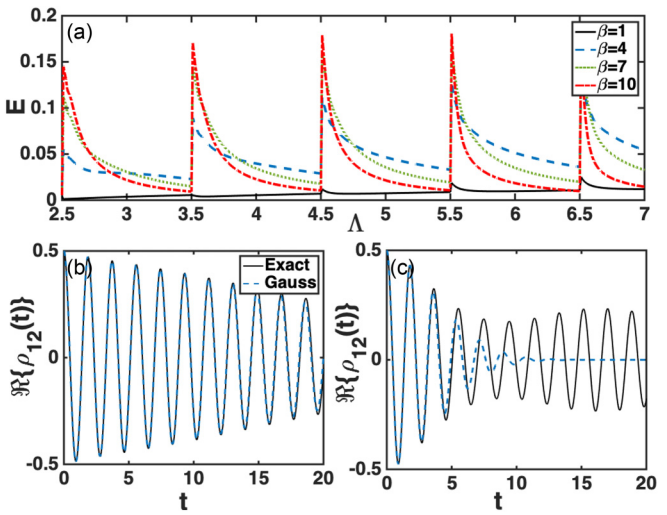

FIG. 6. (a) Time-averaged error between the Gaussian evolution and the exact one, for $\eta = 0.01$ and several temperatures $\beta = 1, 4, 7, 10$ corresponding to black solid, blue dashed, green dotted, and red dot-dashed lines, respectively. The maximal time taken is $T = 20$, which corresponds to the time up to which, for the harmonic case, the system evolves without any border effect. Also shown is the evolution of the real part of the off-diagonal elements of the density matrix as predicted by the exact map (black solid line) and the Gaussian-approximated one (blue dashed line) for $\beta = 7$ and (b) $\Lambda = 2.5$ and (c) $\Lambda = 2.6$.

degree of anharmonicity. First, we analyzed the variation of the dephasing time with the anharmonic parameter of the environment Λ and found the following.

(i) On a coarse-grained scale in Λ, the decoherence time increases towards both the harmonic and anharmonic limits. In the anharmonic limit the decoherence is slow due to the few bound states in the environment. When the anharmonicity grows this effect is compensated by the fact that the environment correlation function does not decay to zero, but to a real value, the offset. Such an offset occurs due to the presence of bound states $|p\rangle$ that are highly asymmetric, i.e., for which $\langle p|x_k|p\rangle > 0$, where x_k is the displacement operator with respect to the potential minimum. Hence, the offset becomes negligible towards the harmonic limit, which explains the slowing down of the dephasing.

(ii) On a finer scale, for a given integer number n there are two different regions in Λ: type I regions where $\Lambda = n + \frac{1}{2} - \epsilon$, with ϵ small, where we have an integer number of bound states $N = n$ that are all strongly bounded, i.e., energetically far from the dissociation limit, and type II regions for $\Lambda = n + \frac{1}{2} + \epsilon$, with ϵ small, where we have $N = n + 1$ bound states and the highest-energy one $|m\rangle$ is weakly bounded. The displacement of such a weakly bounded state with respect to the center of the potential is large, leading to an overlap $\langle n|x_k|n\rangle \gg 1$ that produces a particularly large offset and thus a very strong dephasing in those regions.

Second, we analyzed the non-Markovianity or backflow of information and found that it only occurs at high anharmonicities and that it is concentrated in type II regions. Moreover, the backflow is only relevant at low temperatures, which suggests that while it is indeed linked to a large anharmonicity, it is nevertheless hindered by the presence of the offset. Indeed, at high temperatures such an offset becomes dominant and gives rise to a dephasing dynamics that is too fast to allow for backflow.

A similar situation occurs when considering how relevant or necessary it is to account for the non-Gaussianity of the bath. To check this we consider the correlation function of the bath and build the corresponding Gaussian map to compare it with the exact non-Gaussian one. As it turns out, for high temperatures the effect of the non-Gaussianity becomes negligible and both exact and Gaussian versions give approximately the same dynamics. Indeed, the offset is also present in the Gaussian version of the map and is so large that it dominates the decay. The non-Gaussianity, and therefore the effect of the higher-order moments, starts to be important for lower temperatures, when the offset is not so relevant but still a large anharmonicity is present. In addition, the Gaussian analog map predicts no backflow in any regime, which reinforces the idea that the backflow is related to the anharmonicity and non-Gaussian character of the bath.

Overall, this analysis has revealed the presence of a variety of dynamical regimes for an impurity coupled to an anharmonic environment, which depend not only on the number of bound states in the environment $|m\rangle$ but also on their location within the anharmonic potential and therefore on their degree of asymmetry. While the relevance of each of these regimes and situations remains to be determined and analyzed in each physical situation and specific model, this study systematically discussed how rich the dynamics of an open system may become when smoothly going beyond the standard harmonic bath situation. In this context, concepts such as environment size effects, the origin and nature of the information backflow [48], and other related concepts such as divisibility [49], the existence of a dynamical equation, i.e., invertibility of the map [41,45], or validity of the weak-coupling approximation may need to be revisited and further analyzed in the future.

ACKNOWLEDGMENTS

The authors acknowledge D. Wierichs, C. Parra, A. Recati, C. Hubig, Christiane Koch, N. O. Linden, and U. Schollwöck for interesting discussions. This research was supported financially by DFG Grant No. GZ: VE 993/1-1 and in part by the National Science Foundation under Grant No. NSF PHY-1748958.

APPENDIX A: BOUND STATES OF MORSE OSCILLATORS

We discuss in this Appendix how to derive the bound states of the Morse potential. To this aim, we will follow the derivations in [36] but describe in more detail some of the steps that in the original paper were only sketched. In addition, we will put more emphasis on the criteria to decide whether a solution is physical or not. We start with the Hamiltonian

$$H = \frac{p^2}{2m} + D(e^{-2\alpha x} - 2e^{-\alpha x}). \tag{A1}$$

We will now do a few transformations in order to solve the stationary Schrödinger equation related to this Hamiltonian. First we define $x' := \alpha x$, leading to

$$H' = -\frac{\hbar^2\alpha^2}{2m}\partial_{x'}^2 + D(e^{-2x'} - 2e^{-x'}). \tag{A2}$$

Now we rescale this to make the Hamiltonian dimensionless: $H_0 = \frac{2m}{\hbar^2\alpha^2}H'$. Then the Hamiltonian becomes

$$H_0 = -\partial_{x'}^2 + D'(e^{-2x'} - 2e^{-x'}), \tag{A3}$$

with $D' = \frac{2m}{\hbar^2\alpha^2}D := (N + \frac{1}{2})^2$. From now on we will omit the primes. The bound states $\psi(x)$ for the energy $E < 0$ must fulfill the following:

$$-\partial_x^2\psi(x) + \left(N + \tfrac{1}{2}\right)^2(e^{-2x} - 2e^{-x})\psi(x) - E\psi(x) = 0.$$

In order to make this a linear differential equation we substitute $z = (2N + 1)\exp(-x)$, which leads us to

$$z^2\partial_z^2\psi(z) + z\partial_z\psi(z) + \left[E + \left(N + \tfrac{1}{2}\right)z - \tfrac{1}{4}z^2\right]\psi(z) = 0.$$

Now we substitute $\psi(z) = z^{b/2}\exp(-az)F(z)$. After a rather long but straightforward calculation this results in

$$z\partial_z^2F(z) + (-2az + b + 1)\partial_zF(z) + \left(a^2 - \frac{1}{4}\right)zF(z) + \left[-ba - a + \left(N + \frac{1}{2}\right)\right]F(z) + \left(E + \frac{b^2}{4}\right)\frac{1}{z}F(z) = 0. \tag{A4}$$

In order to simplify this equation we choose $a = \frac{1}{2}$ and $b^2 = -4E$. With this choice we obtain

$$z\partial_z^2 F(z) + (b+1-z)\partial_z F(z) + \left[-\frac{b}{2} - \frac{1}{2} + \left(N + \frac{1}{2}\right)\right] F(z) = 0. \tag{A5}$$

This is the Laguerre equation

$$zy'' + (1+b-z)y' + \lambda y = 0. \tag{A6}$$

As discussed in [36], one set of solutions for this equation are the Laguerre polynomials, and indeed these are the only polynomial solutions. In the original paper other possible solutions are immediately discarded as unphysical. In the following we will give proof that this is the case, which justifies the approach in [36].

Hence we start with the series ansatz

$$y(z) = \sum_{n=0}^{\infty} a_n z^n. \tag{A7}$$

Inserting this into the Laguerre equation gives us

$$\sum_{n=2}^{\infty} a_n n(n-1) z^{n-1} + \sum_{n=1}^{\infty} a_n n(1+b) z^{n-1} - \sum_{n=1}^{\infty} a_n n z^n + \sum_{n=0}^{\infty} \lambda a_n z^n = 0. \tag{A8}$$

Shifting the indices in the first two sums gives

$$\sum_{n=1}^{\infty} n[a_{n+1}(n+1) - a_n] z^n + \sum_{n=0}^{\infty} [a_{n+1}(n+1)(1+b) + \lambda a_n] z^n = 0. \tag{A9}$$

Thus, for $n = 0$ we obtain the following relation between the first two coefficients:

$$a_1 = \frac{-\lambda}{1+b} a_0. \tag{A10}$$

For $n > 0$ we then obtain the recurrence relation

$$a_{n+1} = \frac{-\lambda + n}{(n+1)(1+b+n)} a_n. \tag{A11}$$

Iterating this equation gives us

$$a_n = \frac{(-\lambda)_n}{(1+b)_n n!} a_0, \tag{A12}$$

where $(x)_n$ is the Pochhammer symbol defined as

$$(x)_n = \Gamma(x+n)/\Gamma(x), \tag{A13}$$

which is equivalent to $(x)_n = \prod_{l=0}^{n-1}(x+l)$. Note that, because of the definition of the Pochhammer symbols, the series terminates if λ is a non-negative integer. This leaves us with two cases: One is that λ is a non-negative integer and the other one is when this is not the case. We first investigate the case where λ is not a non-negative integer. We now show that in this case we do not obtain physical solutions of the Schrödinger equation. The argument is that if the series does not terminate, then the wave function will not be normalizable and will therefore not represent a physical bound state. One can see this by splitting the series into a polynomial and a nonpolynomial part and then approximating the behavior of the nonpolynomial part. The solution of the Laguerre equation is

$$y(z) = a_0 \sum_{n=0}^{\infty} \frac{(-\lambda)_n}{(1+b)_n n!} z^n. \tag{A14}$$

First of all, we note that, without loss of generality, we can say that there exists an N such that for all $n>N$, $-\lambda+N+n>0$. Now we split the sum as

$$y(z) = a_0 \sum_{n=0}^{N} \frac{(-\lambda)_n}{(1+b)_n n!} z^n + a_0 \sum_{n=N+1}^{\infty} \frac{(-\lambda)_n}{(1+b)_n n!} z^n.$$

We can restrict ourselves to $b > 0$, since if $b < 0$ then we would have a singularity in the wave function due to the substitution we made earlier. This would make it unphysical. With this the coefficients in the second sum all have the same sign. The first sum is just a polynomial and cannot give us any problems, because in our substitution from earlier we have a term that scales as $\exp(-z/2)$. That is why we abandon the polynomial part in this consideration. Now if $-\lambda > 1 + b$ then we are already done, because then the following holds:

$$\begin{aligned} \left| a_0 \sum_{n=N+1}^{\infty} \frac{(-\lambda)_n}{(1+b)_n n!} z^n \right| &= a_0 \sum_{n=N+1}^{\infty} \left| \frac{(-\lambda)_n}{(1+b)_n n!} \right| z^n \\ &> a_0 \sum_{n=N+1}^{\infty} \frac{z^n}{n!} \\ &= a_0 e^z - a_0 \sum_{n=0}^{N} \frac{z^n}{n!}. \end{aligned} \tag{A15}$$

The first equality holds because we are only interested in the solution for z in $[0, \infty)$. This means that in the case where $-\lambda > 1 + b$ the solution scales even stronger in z than $\exp(z)$ and thus it is unphysical, because neither our factor of $\exp(-z/2)$ nor any polynomial can compete with that. So now let us see how this goes for $-\lambda < 1 + b$. In this case this is a bit more difficult. First we need to note that $\lim_{n\to\infty}(-\lambda + n)/(1 + b + n) = 1$. This means for all $\epsilon > 0$ there exists an N' such that for all $n \geqslant N'$,

$$\left| \frac{-\lambda + n}{1+b+n} - 1 \right| < \epsilon, \tag{A16}$$

from which it follows that for $n \geqslant N'$, $\frac{-\lambda+n}{1+b+n} > 1 - \epsilon$. With this we can investigate the nonpolynomial part further:

$$a_0 \sum_{n=N+1}^{\infty} \frac{(-\lambda)_n}{(1+b)_n n!} z^n = a_0 \sum_{n=N+1}^{N'} \frac{(-\lambda)_n}{(1+b)_n n!} z^n + a_0 \sum_{n=N'+1}^{\infty} \frac{(-\lambda)_n}{(1+b)_n n!} z^n.$$

Now let us just look at the nonpolynomial part again:

$$\sum_{n=N'+1}^{\infty}\frac{(-\lambda)_n}{(1+b)_n n!}z^n = c_{N'}\sum_{n=N'+1}^{\infty}\left(\prod_{l=0}^{n-1}\frac{-\lambda+N'+l}{1+b+N'+l}\right)\frac{z^n}{n!}$$
$$> c_{N'}\sum_{n=N'+1}^{\infty}\left(\prod_{l=0}^{n-1}(1-\epsilon)\right)\frac{z^n}{n!}$$
$$= c_{N'}e^{(1-\epsilon)z} - c_{N'}\sum_{n=0}^{N'}(1-\epsilon)^n\frac{z^n}{n!}. \quad \text{(A17)}$$

Here $c_{N'} := \frac{(-\lambda)_{N'}}{(1+b)_{N'}}$ and ϵ can be chosen to be any positive real number. Thus if one chooses, for example, $\epsilon = \frac{1}{4}$ one can see that the wave function is not normalizable. Again, the second term does not make it normalizable, since it is just a polynomial. With this extensive proof we show that the only physical solutions are obtained for λ being a non-negative integer. With this we obtain an equation for b and for the energy since $b^2/4 = -E$:

$$n = N - \frac{b}{2}, \quad \text{(A18)}$$

$$b = 2N - 2n, \quad \text{(A19)}$$

$$E_n = -(N-n)^2. \quad \text{(A20)}$$

Here $\lambda \to n$ is a non-negative integer. Recall that b is only allowed to be positive, because otherwise either the wave functions or the probability density will have a singularity at $z = 0$. This means that if N is an natural number it is the number of bound states; if not, then the integer part of $N+1$ is the number of bound states. The wave function is then given by

$$\psi_n(z) = z^{2N-2n}e^{-z/2}y_n^{2N-2n}(z)$$
$$= z^{2N-2n}e^{-z/2}\sum_{m=0}^{n}\frac{(-n)_m}{(2N-2n+1)_m m!}z^m$$
$$= z^{2N-2n}e^{-z/2}\sum_{m=0}^{n}(-1)^m\binom{n}{m}\frac{z^m\Gamma(2N-2n+1)}{\Gamma(2N-2n+1+m)}. \quad \text{(A21)}$$

With proper normalization this becomes

$$\psi_n(z) = N_n z^{2N-2n}e^{-z/2}\sum_{m=0}^{n}(-1)^m\binom{n}{m}$$
$$\times\frac{z^m}{\Gamma(2N-2n+1+m)}. \quad \text{(A22)}$$

Here we have defined z and N_n as follows:

$$z = (2N+1)\exp(-x), \quad \text{(A23)}$$

$$N_n = \sqrt{\frac{(2N-2n)\Gamma(v_n^N)}{n!}}. \quad \text{(A24)}$$

Note that all these equations are still for a dimensionless Hamiltonian. When we reintroduce the parameters we rescaled the Hamiltonian with in the beginning we get

$$E_n = -\frac{\hbar^2\alpha^2}{2m}(N-n)^2$$
$$= -\frac{\hbar^2\alpha^2}{2m}\left[\Lambda^2 + \left(n+\frac{1}{2}\right)^2 - 2\Lambda\left(n+\frac{1}{2}\right)\right], \quad \text{(A25)}$$

where Λ is defined as $\Lambda := N + \frac{1}{2}$. Now for a given Morse oscillator we want the part that is proportional to $n + \frac{1}{2}$ to be the harmonic part; thus it should be $\hbar\omega(n+\frac{1}{2})$. So now we change the parameters of the Morse oscillator from α and D to ω and Λ:

$$\alpha := \sqrt{\frac{m\omega}{\hbar\Lambda}}, \quad \text{(A26)}$$

$$D := \frac{\hbar\omega\Lambda}{2}. \quad \text{(A27)}$$

As mentioned earlier, we obtain a set $\{\omega_k, g_k\}$ by discretizing the spectral density. The ω in the above equations corresponds to the ω_k that we obtain by the discretization. For the implementation of the Morse environment we choose Λ to be constant for all oscillators, and thus they all have the same number of bound states.

APPENDIX B: MATRIX ELEMENTS OF THE POSITION OPERATOR

In our description, it is highly convenient to write the Morse Hamiltonian in its diagonal form. This in turn means that the interaction Hamiltonian should also be expressed in such a basis. To this aim, it is necessary to write the matrix element of the position operator in such a basis, a computation that, as we will see in the following, is not at all trivial. To proceed with it, we make use of the wave function of the bound states, as computed in Appendix A. In the following, we consider the same strategy as in Ref. [50], that is we compute them as

$$\langle n|x|m\rangle = \lim_{\eta\to 0}\mathrm{Im}\left(\frac{d}{d\eta}\langle n|\exp(i\eta x)|m\rangle\right). \quad \text{(B1)}$$

Here x is still supposed to be dimensionless, and thus the rescaling of Appendix A is still in place. Actually, computing $\langle n|\exp(i\eta x)|m\rangle$ is pretty straightforward apart from the fact that one has to use the Gaussian hypergeometric theorem and the Saalschütz theorem. Those will both be stated when we use them. Nevertheless, the most delicate part of the computation is taking the limit after the derivative. Since this important step was not detailed in [50], we will present it here in more detail.

Let us first consider that $\exp(i\eta x) = (2N+1)^{i\eta}z^{-i\eta}$ such that

$$\langle n|\exp(i\eta x)|m\rangle = \int_{-\infty}^{\infty}dx\,\psi_n^*(z)\psi_m(z)(2N+1)^{i\eta}z^{-i\eta}$$
$$= \int_0^{\infty}dz\,\psi_n^*(z)\psi_m(z)(2N+1)^{i\eta}z^{-i\eta-1}.$$

Then, considering the wave functions (A22), we can now compute

$$\langle n|\exp(i\eta x)|m\rangle = (2N+1)^{i\eta}N_nN_m\sum_{n',m'=0}^{n,m}\binom{n}{n'}\binom{m}{m'} \times(-1)^{n'+m'}\frac{1}{\Gamma\left(u^N_{nn}+n'+1\right)\Gamma\left(u^N_{mm}+m'+1\right)} \times\int_0^\infty dz\, e^{-z}z^{u^N_{nm}+n'+m'-i\eta-1}, \tag{B2}$$

where we have defined

$$u^N_{nm}=2N-n-m,\quad v^N_n=2N-n+1. \tag{B3}$$

Using the definition of the Γ function, $\Gamma(z)=\int_0^\infty dt\, e^{-t}t^{z-1}$, we obtain

$$\langle n|\exp(i\eta x)|m\rangle = (2N+1)^{i\eta}N_nN_m\sum_{n'=0}^{n}\frac{\Sigma(m,n,\eta)}{\Gamma\left(u^N_{nn}+n'+1\right)}, \tag{B4}$$

where we have defined a function that contains all terms that depend on m',

$$\Sigma(m,n,\eta):=\sum_{m'=0}^{m}\binom{m}{m'}(-1)^{m'}\frac{\Gamma\left(u^N_{nm}+n'+m'-i\eta\right)}{\Gamma\left(u^N_{mm}+m'+1\right)}. \tag{B5}$$

We now consider that

$$(-m)_{m'}=\prod_{l=0}^{m'-1}(-m+l)=(-1)^{m'}\frac{m!}{(m-m')!} \tag{B6}$$

in order to reexpress Eq. (B5) in terms of Pochhammer symbols (A13),

$$\Sigma(m,n,\eta):=\sum_{m'=0}^{m}\frac{\Gamma\left(u^N_{nm}+n'-i\eta\right)}{\Gamma\left(u^N_{mm}+1\right)} \times\frac{\left(u^N_{nm}+n'-i\eta\right)_{m'}(-m)_{m'}}{\left(u^N_{mm}+1\right)_{m'}m'!}. \tag{B7}$$

This allows us to perform the sum over m' by using the Gaussian hypergeometric theorem, which states that (see [50], Sec. 3.1)

$$\sum_{m'=0}^{\infty}\frac{(a)_{m'}(b)_{m'}}{(c)_{m'}m'!}=\frac{\Gamma(c)\Gamma(c-a-b)}{\Gamma(c-a)\Gamma(c-b)}. \tag{B8}$$

Note that $(-m)_{m'}$ becomes 0, when $m'>m$, which allows us to apply the theorem even though it is meant for summation up to infinity. When using this we obtain

$$\Sigma(n,m,\eta)=\frac{\Gamma\left(u^N_{nm}+n'-i\eta\right)\Gamma(n-n'+1+i\eta)}{\Gamma(n-m+1-n'+i\eta)\Gamma\left(v^N_m\right)}.$$

Thus the matrix element becomes

$$\langle n|\exp(i\eta x)|m\rangle = \frac{(2N+1)^{i\eta}N_nN_m}{\Gamma\left(v^N_m\right)}\sum_{n'=0}^{n}\binom{n}{n'}(-1)^{n'} \times\frac{\Gamma\left(u^N_{nm}+n'-i\eta\right)\Gamma(n-n'+1+i\eta)}{\Gamma(n-m+1-n'+i\eta)\Gamma\left(u^N_{nn}+n'+1\right)}. \tag{B9}$$

We want to organize this expression into two terms, where one contains everything depending on n'. Also, we want to have the things that depend on n' to be formulated in terms of Pochhammer symbols again so that we can ultimately use the Saalschütz theorem. First we note the following:

$$\Gamma(a)=(-1)^{n'}(-a+1)_{n'}\Gamma(a-n'). \tag{B10}$$

With this we obtain

$$\langle n|\exp(i\eta x)|m\rangle = A_{mn}(\eta)\Gamma_{mn}(\eta), \tag{B11}$$

where $A_{mn}(\eta)$ and $\Gamma_{mn}(\eta)$ are defined as

$$A_{mn}(\eta)=\frac{(2N+1)^{i\eta}N_nN_m}{\Gamma\left(v^N_m\right)}\frac{\Gamma\left(u^N_{nm}-i\eta\right)\Gamma(n+1+i\eta)}{\Gamma(n-m+1+i\eta)\Gamma\left(u^N_{nn}+1\right)},$$
$$\Gamma_{mn}(\eta)={}_3F_2\left(-n+m-i\eta,\,u^N_{nm}-i\eta,\,-n;\,u^N_{nn}+1,\,-n-i\eta;\,1\right), \tag{B12}$$

where ${}_3F_2$ is a generalized hypergeometrical function, as can also be seen in [50] [Sec. 3.1, Eq. (18)] and [51] (Chap. 4). The derivative can now be computed as

$$\frac{d}{d\eta}\langle n|\exp(i\eta x)|m\rangle = \left(\frac{d}{d\eta}A_{mn}\right)(\eta)\Gamma_{mn}(\eta)+A_{mn}(\eta)\left(\frac{d}{d\eta}\Gamma_{mn}\right)(\eta). \tag{B13}$$

Up to now we went pretty much along the lines of [50], apart from expressing things in a much more detailed manner of course. Taking this derivative and the limit afterward is the most problematic part of this computation, and since this step was skipped in [50] we are going to do it in full detail here.

Let us distinguish two cases: the off-diagonal elements, namely, $m>n$, and the diagonal elements. Note that the condition $m>n$ does not imply a loss of generality since x is Hermitian. First we take a look at the off-diagonal elements. For $m>n$ one can see that in the denominator of $A_{mn}(\eta)$ there is a term $\Gamma(n-m+1+i\eta)$ which approaches a singularity in the limit $\eta\to 0$. Thus $A_{mn}(\eta)$ becomes 0 in the limit. If $\frac{d}{d\eta}\Gamma_{nm}(\eta)$ does not have a diverging term in the limit this means that we only have to take into account the term containing the derivative of $A_{mn}(\eta)$. By looking at the form of $\Gamma_{mn}(\eta)$ we can already see that taking a derivative and sending η to 0 will not give us something divergent. Thus we only care about the derivative of $A_{mn}(\eta)$,

$$\lim_{\eta\to0}\frac{d}{d\eta}A_{mn}(\eta)=\frac{(2N+1)^{i\eta}N_nN_m\Gamma(n+1)\Gamma\left(u^N_{nm}\right)}{\Gamma\left(v^N_m\right)\Gamma\left(u^N_{nn}+1\right)} \times(-i)\lim_{\eta\to0}\frac{\psi(n-m+1+i\eta)}{\Gamma(n-m+1+i\eta)}, \tag{B14}$$

where $\psi(x):=\frac{d}{dx}\ln[\Gamma(x)]=\frac{\frac{d}{dx}\Gamma(x)}{\Gamma(x)}$ is the digamma function. Here we skipped a few steps, but they are just taking the derivative and realizing that in the limit $\eta\to0$ only this term survives, because in all the other terms there is no singularity in the enumerator. In order to obtain this limit one can perform a nice trick, namely one can use the two identities [see [51], Chap. 1.2, Eq. (6) and Chap. 1.7, Eq. (11)]

$$\Gamma(z)\Gamma(1-z)=\pi\csc(\pi z), \tag{B15}$$

$$\psi(1-z)-\psi(z)=\pi\cot(\pi z). \tag{B16}$$

With the use of these equations, the limit becomes

$$\lim_{\eta\to 0}\frac{\psi(n-m+1+i\eta)}{\Gamma(n-m+1+i\eta)} = -\cos[\pi(n-m+1)]\Gamma(m-n) = (-1)^{m-n}\Gamma(m-n). \tag{B17}$$

With this we obtain (for $m > n$)

$$\lim_{\eta\to 0}\frac{d}{d\eta}A_{mn}(\eta) = i(-1)^{m-n+1}\frac{N_nN_m\Gamma(n+1)}{\Gamma\left(v_m^N\right)\Gamma\left(u_{nn}^N+1\right)} \times\Gamma\left(u_{nm}^N\right)\Gamma(m-n). \tag{B18}$$

Thus the only thing that remains to be done in the off-diagonal case is to take the limit for $\Gamma_{mn}(\eta)$. If we take this limit we obtain

$$\lim_{\eta\to 0}\Gamma_{mn}(\eta) = {}_3F_2\left(-n+m, u_{nm}^N, -n; u_{nn}^N+1, -n; 1\right).$$

A generalized hypergeometric function ${}_3F_2$ is Saalschützian if its parameters are in the following form, stated by the Saalschütz theorem (see [51], Chap. 4.4):

$${}_3F_2(a,b,-n;c,1+a+b-c-n,1) = \frac{(c-a)_n(c-b)_n}{(c)_n(c-a-b)_n}. \tag{B19}$$

In the limit $\eta\to 0$ the parameters for our generalized hypergeometric function are of exactly that form, and thus

$$\lim_{\eta\to 0}\Gamma_{mn}(\eta) = \frac{(-m)_n(-2N+m)_n}{(-n)_n(-2N-n)_n}. \tag{B20}$$

Here we have considered that

$$(-x)_n = \prod_{l=0}^{n-1}(-x+j) = (-1)^n\frac{\Gamma(x+1)}{\Gamma(x-n+1)}. \tag{B21}$$

With this we obtain

$$\lim_{\eta\to 0}\Gamma_{mn}(\eta) = \frac{m!\Gamma\left(v_m^N\right)\Gamma\left(u_{nn}^N+1\right)}{n!\Gamma\left(v_n^N\right)\Gamma\left(u_{nm}^N+1\right)\Gamma(m-n+1)}.$$

Now we can finally obtain the matrix elements for the off-diagonal term with $m > n$:

$$\langle n|x|m\rangle = \frac{(-1)^{m-n+1}m!N_nN_m\Gamma\left(u_{nm}^N\right)\Gamma(m-n)}{\Gamma\left(v_n^N\right)\Gamma\left(u_{nm}^N+1\right)\Gamma(m-n+1)} = \frac{2(-1)^{m-n+1}}{u_{nm}^N(m-n)}\sqrt{\frac{m!(N-n)(N-m)\Gamma\left(v_m^N\right)}{n!\Gamma\left(v_n^N\right)}}.$$

The two preceding lines show our result for the off-diagonal elements. Now for the diagonal elements $A_{mn}(\eta)$ does not have a singularity in the denominator, and thus both terms contribute. Let us first compute the contribution from $A_{nn}(\eta)$:

$$\lim_{\eta\to 0}\frac{d}{d\eta}A_{nn}(\eta) = i\ln(2N+1) - i\psi\left(u_{nn}^N\right) + i\psi(n+1) - i\psi(1). \tag{B22}$$

Here we have not detailed the derivation, which basically consists in taking the derivative of each term of $A_{nn}(\eta)$ in Eq. (B12) and then taking the limit. Note that the derivation of $\lim_{\eta\to 0}\Gamma_{nm}(\eta)$ was not relying on $m > n$, so it also holds here, and thus $\lim_{\eta\to 0}\Gamma_{nn}(\eta) = 1$. So now comes the tricky part. In order to obtain a nice form for the derivative of $\Gamma_{nn}(\eta)$ we would like to use the Saalschütz theorem of Eq. (B19); however, if we are not in the limit where $\eta\to 0$ our ${}_3F_2$ is not Saalschützian. This is where we use a trick. We define another $\tilde{\Gamma}_{nn}(\eta)$ that is Saalschützian and that has the same derivative in the limit $\eta\to 0$. We define $\tilde{\Gamma}_{nn}(\eta)$ as follows:

$$\tilde{\Gamma}_{nn}(\eta) := {}_3F_2\left(-i\eta, u_{nn}^N-i\eta, -n; u_{nn}^N+1-i\eta, -n-i\eta; 1\right).$$

First we have to check that in the limit of $\eta\to 0$ this indeed has the same derivative as $\Gamma_{nn}(\eta)$. So let us take a look at how this is expressed in terms of Pochhammer symbols:

$$\tilde{\Gamma}_{nn}(\eta) = \sum_{n'=0}^{n}\frac{(-i\eta)_{n'}\left(u_{nn}^N-i\eta\right)_{n'}(-n)_{n'}}{\left(u_{nn}^N+1-i\eta\right)_{n'}(-n-i\eta)_{n'}}. \tag{B23}$$

Because of the term $(-i\eta)_{n'}$, this is proportional to η, so the only term that contributes to the derivative in the limit of $\eta\to 0$ is the one where one takes the derivative of $(-i\eta)_{n'}$ [in other words, the derivative of the other terms with η will always be multiplied by $(-i\eta)_{n'}$ and therefore vanish in the limit $\eta\to 0$]. This leads to

$$\lim_{\eta\to 0}\frac{d}{d\eta}\tilde{\Gamma}_{nn}(\eta) = \lim_{\eta\to 0}\sum_{n'=0}^{n}\frac{\left[\frac{d}{d\eta}(-i\eta)_{n'}\right]\left(u_{nn}^N-i\eta\right)_{n'}(-n)_{n'}}{\left(u_{nn}^N+1-i\eta\right)_{n'}(-n-i\eta)_{n'}} = \sum_{n'=0}^{n}\frac{\lim_{\eta\to 0}\left[\frac{d}{d\eta}(-i\eta)_{n'}\right]\left(u_{nn}^N\right)_{n'}(-n)_{n'}}{\left(u_{nn}^N+1\right)_{n'}(-n)_{n'}}.$$

Now let us compare this to $\Gamma_{nn}(\eta)$:

$$\Gamma_{nn}(\eta) = \sum_{n'=0}^{n}\frac{(-i\eta)_{n'}\left(u_{nn}^N-i\eta\right)_{n'}(-n)_{n'}}{\left(u_{nn}^N+1\right)_{n'}(-n-i\eta)_{n'}}. \tag{B24}$$

With the same argument as for $\tilde{\Gamma}_{nn}(\eta)$ we obtain

$$\lim_{\eta\to 0}\frac{d}{d\eta}\Gamma_{nn}(\eta) = \sum_{n'=0}^{n}\frac{\lim_{\eta\to 0}\left[\frac{d}{d\eta}(-i\eta)_{n'}\right]\left(u_{nn}^N\right)_{n'}(-n)_{n'}}{\left(u_{nn}^N+1\right)_{n'}(-n)_{n'}} = \lim_{\eta\to 0}\frac{d}{d\eta}\tilde{\Gamma}_{nn}(\eta). \tag{B25}$$

Now we use the Saalschütz theorem to compute $\tilde{\Gamma}_{nn}(\eta)$:

$$\tilde{\Gamma}_{nn}(\eta) = \frac{\left(u_{nn}^N+1\right)_n(1)_n}{\left(u_{nn}^N+1-i\eta\right)_n(1+i\eta)_n} = \frac{\Gamma\left(v_n^N\right)\Gamma(1+n)\Gamma\left(u_{nn}^N+1-i\eta\right)\Gamma(1+i\eta)}{\Gamma\left(u_{nn}^N+1\right)\Gamma\left(v_n^N-i\eta\right)\Gamma(1+i\eta+n)}. \tag{B26}$$

Thus

$$\lim_{\eta\to 0}\frac{d}{d\eta}\tilde{\Gamma}_{nn}(\eta) = -i\psi\left(u_{nn}^N+1\right) + i\psi(1) + i\psi\left(v_n^N\right) - i\psi(1+n). \tag{B27}$$

Also note that $\lim_{\eta\to 0}A_{nn}(\eta) = 1$. With this we can compute the diagonal matrix elements

$$\langle n|x|n\rangle = \mathrm{Im}\left(\lim_{\eta\to 0}\frac{d}{d\eta}A_{nn}(\eta) + \lim_{\eta\to 0}\frac{d}{d\eta}\Gamma_{nn}(\eta)\right) = \ln(2N+1) - \psi\left(u_{nn}^N\right) - \psi\left(u_{nn}^N+1\right) + \psi\left(v_n^N\right). \tag{B28}$$

For the sake of completeness let us state the off-diagonal elements for $m > n$ here again:

$$\langle n|x|m\rangle = \frac{2(-1)^{m-n+1}}{u^N_{nm}(m-n)}\sqrt{\frac{m!(N-n)(N-m)\Gamma\left(v^N_m\right)}{n!\Gamma\left(v^N_n\right)}}.$$

We still refer to the dimensionless x, and thus in order to obtain the matrix elements of $b^\dagger + b$ we only have to rescale the ones from (B28) and (B29) by a factor $\sqrt{2/\Lambda}$, namely,

$$b^\dagger + b = \sqrt{\frac{2m\omega}{\alpha\hbar}}x = \sqrt{\frac{2}{\Lambda}}x. \tag{B29}$$

[1] H. Breuer and F. Petruccione, *The Theory of Quantum Open Systems* (Oxford University Press, Oxford, 2002).
[2] T. Brandes, Phys. Rep. **408**, 315 (2005).
[3] Á. Rivas and S. F. Huelga, *Open Quantum Systems: An Introduction* (Springer, Heidelberg, 2011).
[4] Á. Rivas, S. F. Huelga, and M. B. Plenio, Rep. Prog. Phys. **77**, 094001 (2014).
[5] H.-P. Breuer, E.-M. Laine, J. Piilo, and B. Vacchini, Rev. Mod. Phys. **88**, 021002 (2016).
[6] I. de Vega and D. Alonso, Rev. Mod. Phys. **89**, 015001 (2017).
[7] R. Feynman and F. Vernon, Jr., Ann. Phys. (NY) **24**, 118 (1963).
[8] A. J. Leggett, S. Chakravarty, A. T. Dorsey, M. P. A. Fisher, A. Garg, and W. Zwerger, Rev. Mod. Phys. **59**, 1 (1987).
[9] J. B. Gilmore and R. H. McKenzie, Chem. Phys. Lett. **421**, 266 (2006).
[10] A. Nazir, Phys. Rev. Lett. **103**, 146404 (2009).
[11] D. Xu and K. Schulten, Chem. Phys. **182**, 91 (1994).
[12] M. Plenio and S. Huelga, New J. Phys **10**, 113019 (2008).
[13] A. Ishizaki and G. Fleming, J. Chem. Phys. **130**, 23411 (2009).
[14] P. Rebentrost, M. Mohseni, I. Kassal, and S. A.-G. A. Lloyd, New J. Phys. **11**, 033003 (2009).
[15] I. de Vega, J. Phys. B **44**, 245501 (2011).
[16] M. Mohseni, A. Shabani, S. Lloyd, Y. Omar, and H. Rabitz, J. Chem. Phys. **138**, 204309 (2013).
[17] J. Tang, J. Chem. Phys. **98**, 6263 (1993).
[18] P. F. Barbara, T. J. Meyer, and M. A. Ratner, J. Phys. Chem. **100**, 13148 (1996).
[19] M. G. Mavros, D. Hait, and T. Van Voorhis, J. Chem. Phys. **145**, 214105 (2016).
[20] J.-L. Brédas, D. Beljonne, V. Coropceanu, and J. Cornil, Chem. Rev. **104**, 4971 (2004).
[21] X. Zhao, W. Shi, L.-A. Wu, and T. Yu, Phys. Rev. A **86**, 032116 (2012).
[22] Y. Tanimura and S. Mukamel, J. Chem. Phys. **99**, 9496 (1993).
[23] K. Okumura and Y. Tanimura, J. Chem. Phys. **105**, 7294 (1996).
[24] D. G. Evans, J. Chem. Phys. **113**, 3282 (2000).
[25] D. M. Lockwood, M. A. Ratner, and R. Kosloff, J. Chem. Phys. **117**, 10125 (2002).
[26] H. Wang and M. Thoss, Chem. Phys. **304**, 121 (2004).
[27] H. Wang and M. Thoss, J. Phys. Chem. A **111**, 10369 (2007).
[28] M. Thoss and H. Wang, Chem. Phys. **322**, 210 (2006).
[29] A. Garg, J. N. Onuchic, and V. Ambegaokar, J. Chem. Phys. **83**, 4491 (1985).
[30] C.-Y. Hsieh and R. Kapral, Entropy **16**, 200 (2014).
[31] N. Prokof'ev and P. Stamp, Rep. Prog. Phys. **63**, 699 (2000).
[32] L. M. Norris, G. A. Paz-Silva, and L. Viola, Phys. Rev. Lett. **116**, 150503 (2016).
[33] Y. Sung, F. Beaudoin, L. M. Norris, F. Yan, D. K. Kim, J. Y. Qiu, U. von Lüepke, J. L. Yoder, T. P. Orlando, L. Viola, S. Gustavsson, and W. D. Oliver, Nat. Commun. **10**, 3715 (2019).
[34] S. López-López, R. Martinazzo, and M. Nest, J. Chem. Phys. **134**, 094102 (2011).
[35] C.-Y. Hsieh and J. Cao, J. Chem. Phys. **148**, 014104 (2018).
[36] P. M. Morse, Phys. Rev. **34**, 57 (1929).
[37] R. S. Burkey and C. D. Cantrell, J. Opt. Soc. Am. B **1**, 169 (1984).
[38] A. K. Kazansky, J. Phys. B **30**, 1401 (1997).
[39] T. Yu and J. H. Eberly, Phys. Rev. B **66**, 193306 (2002).
[40] F. Cosco and S. Maniscalco, Phys. Rev. A **98**, 053608 (2018).
[41] L. Li, M. J. Hall, and H. M. Wiseman, Phys. Rep. **759**, 1 (2018).
[42] A. A. Kananenka, C.-Y. Hsieh, J. Cao, and E. Geva, J. Phys. Chem. Lett. **9**, 319 (2018).
[43] N. Makri, J. Phys. Chem. B **103**, 2823 (1999).
[44] M. Bramberger, C. Parra, and I. de Vega (unpublished).
[45] M. J. W. Hall, J. D. Cresser, L. Li, and E. Andersson, Phys. Rev. A **89**, 042120 (2014).
[46] I. de Vega, U. Schollwöck, and F. A. Wolf, Phys. Rev. B **92**, 155126 (2015).
[47] M. M. Wolf, G. Giedke, and J. I. Cirac, Phys. Rev. Lett. **96**, 080502 (2006).
[48] H.-P. Breuer, E.-M. Laine, and J. Piilo, Phys. Rev. Lett. **103**, 210401 (2009).
[49] Á. Rivas, S. F. Huelga, and M. B. Plenio, Phys. Rev. Lett. **105**, 050403 (2010).
[50] E. F. de Lima and J. E. M. Hornos, J. Phys. B **38**, 815 (2005).
[51] H. Bateman, *Bateman Manuscript Project, Higher Transcendental Functions* (McGraw-Hill, New York, 1953), Vol. 1.